Accurate Double Many-Body Expansion Potential Energy Surface for Ground-State HS2 Based on ab Initio Data Extrapolated to the Complete Basis Set Limit

ARTICLE *in* THE JOURNAL OF PHYSICAL CHEMISTRY A · JUNE 2011

Impact Factor: 2.69 · DOI: 10.1021/jp201980m · Source: PubMed

2 AUTHORS:

Yu-Zhi Song
Shandong Normal University
20 PUBLICATIONS **100** CITATIONS
SEE PROFILE

Antonio J. C. Varandas
University of Coimbra
382 PUBLICATIONS **6,742** CITATIONS
SEE PROFILE

THE JOURNAL OF PHYSICAL CHEMISTRY A

ARTICLE

pubs.acs.org/JPCA

Accurate Double Many-Body Expansion Potential Energy Surface for Ground-State HS_2 Based on ab Initio Data Extrapolated to the Complete Basis Set Limit

Y. Z. Song and A. J. C. Varandas*

Departamento de Química, Universidade de Coimbra, 3004-535 Coimbra, Portugal

Supporting Information

ABSTRACT: A double many-body expansion potential energy surface is reported for the electronic ground state of HS_2 by fitting accurate multireference configuration interaction energies calculated with aug-cc-pV*T*dZ and aug-cc-pV*Q*dZ basis sets upon separate extrapolation of the complete-active-space self-consistent field and dynamical correlation components of the total energy to the complete basis set limit. The major topographical features of the potential energy surface are examined in detail, and the model function is used for thermalized calculations of the rate constants for the $S + SH \rightarrow H + S_2$ reaction at 298 and 400 K. A value of $(1.44 \pm 0.06) \times 10^{-11}$ cm^3 s^{-1} is obtained at 298 K, providing perhaps the most reliable estimate of the rate constant known thus far for such a reaction.

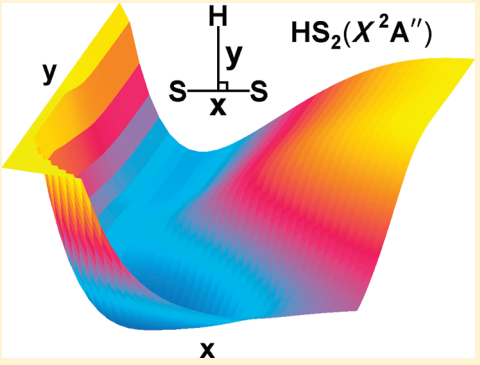

1. INTRODUCTION

The HS_2 radical plays an important role in a variety of environments, notably in combustion and the oxidation of reduced forms of sulfur.[1−4] A vast amount of investigation has been carried out on HS_2 both experimentally and theoretically since the pioneering work by Porter[5] who first proposed that the HS_2 radical was produced during the photolysis of H_2S_2.

The first millimeter-wave spectra of HS_2 reported by Yamamoto and Saito[6] provided the first experimental information about the ground-state structure of HS_2. Isoniemi et al.[7] have subsequently investigated the infrared spectroscopy of the HS_2 radical in an Ar matrix following the 266 nm photolysis of H_2S_2. The absorption bands for two vibrational motions of HS_2 radical, the H−S stretch and the HSS bend, are observed to be 2463 and 903 cm^{-1}. In a recent experiment, Ashworth and Fink[8] have recorded the chemiluminescence spectrum of the HS_2 radical with a high-resolution Fourier-transform spectrometer. The overview spectrum in the region between 4000 and 9000 cm^{-1} has been analyzed, and the thus-obtained vibrational parameters have been presented.

Out of a vast theoretical work, Sannigrahi et al.[9] pioneered the ab initio calculations on the ground and excited states of HS_2, which provided both structural and vibrational information. Owens et al.[10] investigated HX_2 radicals (X = Al, Si, P, and S) using coupled cluster theory, CCSD(T), having reported the equilibrium structure and vibrational frequencies at the global minimum. Later, Denis[11] reported more accurate structural and thermodynamic properties of both ground and excited states of HS_2 and HS_2^+ at the CCSD(T) and B3LYP density functional levels of theory. Moreover, the structural and energetic properties of ground-state HS_2 and HSS → SSH transition state have been examined using the CCSD(T) method by Francisco,[12] who estimated the energy change for the isomerization reaction to be 31.7 ± 1 kcal mol^{-1}. Quite recently, Peterson et al.[13] calculated the equilibrium geometry of the ground and first excited electronic states of HS_2 with highly correlated coupled cluster methods followed by basis set extrapolation. The centrifugal distortion constants, harmonic frequencies, and vibration−rotation coupling constants have then been calculated for both electronic states of HS_2 and DS_2 using accurate three-dimensional, near-equilibrium potential energy and dipole moment functions.

All of the above studies have focused mainly on the structural and spectroscopic constants of the HS_2 radical at its global minimum. Indeed, as far as we are aware, no work toward obtaining a global potential energy surface (PES) for ground-state $HS_2(X^2A'')$ has been reported thus far. In this work, we present a realistic global PES for $HS_2(X^2A'')$ based on double many-body expansion (DMBE)[14−17] theory by accurately fitting the ab initio physically motivated forms to the calculated ab initio energies once extrapolated to the complete basis set (CBS) limit.

This Article is organized as follows. Section 2 describes the ab initio calculations employed in the present work, while section 3 provides a survey of the procedure utilized to CBS extrapolate the calculated energies. The analytical modeling of the DMBE/CBS

Received: March 1, 2011
Revised: April 21, 2011
Published: May 11, 2011

PES is presented in section 4. The major topographical features of the resulting PES are discussed in section 5. Section 6 gathers the concluding remarks.

2. AB INITIO CALCULATIONS

The ab initio calculations are carried out at the multireference configuration interaction level[18,19] of theory, including the popular quasi-degenerate Davidson correction for quadruple excitations [MRCI(Q)],[20] using the full-valence-complete-active space (CASSCF[21]) wave function as reference (abbreviated as CAS). All calculations are performed using the MOLPRO[22] package. The standard aug-cc-pV*X*Z (AV*X*Z) basis set of Dunning[23,24] plus core-polarization high-exponent d functions (AV*X*dZ)[25] has been used for the S atom and AV*X*Z for the H atoms, with $X = T, Q$. A grid of 1601 ab initio points has been chosen to map the PES over the H−S_2 region defined by $3.0 \le R_{S_2}/a_0 \le 4.5$, $2 \le r_{H-S2}/a_0 \le 10$, and $0 \le \gamma/\text{deg} \le 90$. For the S−SH interactions, a grid defined by $2 \le R_{SH}/a_0 \le 4$, $2 \le r_{S-SH}/a_0 \le 10$, and $0 \le \gamma/\text{deg} \le 180$ has been chosen. For both channels, r, R, and γ are the atom−diatom Jacobi coordinates.

3. EXTRAPOLATION TO CBS LIMIT

The ab initio energies calculated in this way have been subsequently extrapolated to CBS limit. To perform the extrapolation, the MRCI(Q) energy is treated in split form by writing:[26]

$$E_X = E_X^{\text{CAS}}(\mathbf{R}) + E_X^{\text{dc}}(\mathbf{R}) \tag{1}$$

where the subscript X indicates that the energy has been calculated in the AV*X*dZ basis, and the superscripts CAS and dc stand as usual for the CAS and dynamical correlation energies, respectively. Note that all extrapolations are carried out pointwise, and hence the vector **R** of the nuclear geometrical coordinates will be omitted for simplicity.

To extrapolate the CAS (uncorrelated in the sense of lacking dynamical correlation) energies, we have followed earlier work[26] by adopting the two-point extrapolation protocol originally proposed by Karton and Martin (KM)[27] to extrapolate the Hartree−Fock energy:

$$E_X^{\text{CAS}} = E_\infty^{\text{CAS}} + B/X^\alpha \tag{2}$$

where α is an effective decay exponent. Being a two-parameter protocol (E_∞^{CAS},B), a minimum of two raw energies will be required for the extrapolation. Specifically, eq 2 will be calibrated from the CAS/AV(T,Q)dZ energy pairs using a value of α = 5.34.

To extrapolate the dynamic correlation (dc) energy, we utilize our own uniform singlet- and triplet-electron pair (USTE[26,28]) scheme, which has already been successfully utilized to construct global DMBE/CBS PESs for $H_2S(X^1A')$[29] and $NH_2(1^2A')$[30] (and partly also for ground-state H_2O[31] as well as jointly with correlation scaling for the quartet ground-state of N_3[32]). It assumes the form:

$$E_X^{\text{dc}} = E_\infty^{\text{dc}} + \frac{A_3}{(X+\alpha)^3} + \frac{A_5}{(X+\alpha)^5} \tag{3}$$

with A_5 being determined by the auxiliary relation:

$$A_5 = A_5(0) + cA_3^{5/4} \tag{4}$$

with the universal-type parameters $A_5(0) = 0.0037685459\ E_h$, $c = -1.17847713\ E_h^{-5/4}$, and $\alpha = -3/8$. Thus, E_∞ and A_3 are the unknowns to be determined from a fit to the dc energies calculated with the AV*T*dZ and AVQdZ basis sets [USTE(T,Q)]. Note that the USTE model suitably calibrated for a specific theory has been shown[26] to yield both the CBS extrapolated full correlation in systems studied by the popular single-reference Møller−Plesset (MP2) and coupled cluster [CCSD and CCSD(T)] methods as well as its dynamical part in MRCI(Q) calculations in very good agreement with the best available estimates. Because the method has been described in detail in various papers ever since its proposal, we refer the reader to ref 33 from which other references can be obtained by cross-referencing.

4. SINGLE-SHEETED DMBE POTENTIAL ENERGY SURFACE

Within the framework of DMBE[14−17] theory, the single-sheeted PES is written as

$$V(\mathbf{R}) = \sum_{i=1}^{3}[V_{\text{EHF}}^{(2)}(\mathbf{R}_i) + V_{\text{dc}}^{(2)}(R_i)] + V_{\text{EHF}}^{(3)}(\mathbf{R}) + V_{\text{ele}}^{(3)}(\mathbf{R}) + V_{\text{dc}}^{(3)}(\mathbf{R}) \tag{5}$$

where $\mathbf{R} = \{R_1,R_2,R_3\}$ is a collective diatomic internuclear separation of triatomic, and the three-body electrostatic term (only present in the presence of overlapping polarizable species) has been separated from the corresponding EHF energy for clarity. Thus, the two-body energy terms are split into two contributions: the extended Hartree−Fock (EHF) and dynamical correlation (dc) energies. Although a similar partition applies to all other n-body energy terms, the electrostatic (ele) long-range contribution has been separated for clarity as noted above, because it varies at long-range with a form akin to three-body dynamical correlation terms. The following subsections give a detailed description of the two-body and three-body energy terms employed in eq 5.

4.1. Two-Body Energy Terms. The diatomic potential energy curves of $S_2(X^3\Sigma_g^-)$ and $SH(X^2\Pi)$ have been calibrated by fitting ab initio energies extrapolated as described in the previous section, having been fitted to an extended Hartree−Fock approximate correlation energy curve, including the united atom limit[34] (EHFACE2U).

The dc energy term assumes the form:[15,34]

$$V_{\text{dc}}^{(2)}(R) = -\sum_{n=6,8,10} C_n\chi_n(R)R^{-n} \tag{6}$$

with the damping functions for the dispersion coefficients assuming the form:

$$\chi_n(R) = [1 - \exp(-A_nR/\rho - B_nR^2/\rho^2)]^n \tag{7}$$

where $A_n = \alpha_0 n^{-\alpha_1}$ and $B_n = \beta_0 \exp(-\beta_1 n)$ in eq 6 are auxiliary functions;[15,17] α_0, β_0, α_1, and β_1 are universal dimensionless parameters for all isotropic interactions: $\alpha_0 = 16.36606$, $\alpha_1 = 0.70172$, $\beta_0 = 17.19338$, and $\beta_1 = 0.09574$. Moreover, ρ is a scaling parameter defined by $\rho/a_0 = 5.5 + 1.25R_0$, where $R_0 = 2(\langle r_X^2\rangle^{1/2} + \langle r_Y^2\rangle^{1/2})$ is the LeRoy[35] parameter, and $\langle r_X^2\rangle$ is the expectation value of squared radius for the outermost electron in atom X ($X = A,B$).

The exponential decaying portion of the EHF-type energy term is written as

$$V_{\text{EHF}}^{(2)}(R) = -\frac{D}{R}\left(1 + \sum_{i=1}^{5} a_i r^i\right)\exp(-\gamma r) \tag{8}$$

dx.doi.org/10.1021/jp201980m |J. Phys. Chem. A 2011, 115, 5274–5283

where

$$\gamma = \gamma_0[1 + \gamma_1 \tan(\gamma_2 r)] \quad (9)$$

$r = R - R_e$ is the displacement from the equilibrium diatomic geometry; D, $a_i(i = 1, ...5)$ and γ_i in eq 8 are adjustable parameters to be obtained as described elsewhere.[15,34]

The numerical values of all of the parameters for both diatomic potentials are gathered in Table 1 of the Supporting Information, while their internuclear dependences are shown in Figure 1. As seen, the modeled potentials mimic accurately the ab initio energies. Equilibrium geometry, vibrational frequencies, and dissociation energy are collected in Table 1. For both S_2 and SH, the dissociation energies increase monotonously as the size of basis sets increases from AV*D*dZ to AV5dZ, and the DMBE/CBS PES gives the deepest well depth. As compared to the CBS results by Peterson et al.,[13] which are extrapolated using CCSD(T)/AV(*Q*,5)dZ energies, our results for the SH diatomic predict a difference of $0.0004a_0$ in the equilibrium geometry, and give vibrational frequencies 0.2 cm^{-1} smaller and dissociation energies only 0.33 kcal mol^{-1} smaller. For the S_2 diatom, the variations are $0.0099a_0$, 0.5 cm^{-1}, and 0.44 kcal mol^{-1}, respectively. This may be considered quite good because we have avoided any expensive MRCI/AV5dZ calculations. As compared to the experimental values, our results also provide an excellent agreement. Table 1 also shows the difference of SH and S_2 dissociation energies $[D_e(S_2) - D_e(SH)]$. The first observation goes to the AV*D*dZ result, which as might be expected is poor, with the AV*T*dZ result still giving an error of more than 4 kcal mol^{-1} when compared to the experimental value. Naturally, the AV*Q*dZ and AV5dZ results show enhanced agreement with experiment, with differences of 2.01 and 0.48 kcal mol^{-1}, respectively. Notably, the DMBE/CBS PES predicts a value of 14.18 kcal mol^{-1}, which differs by 0.77 kcal mol^{-1} from the CBS results by Peterson et al.,[13] and 0.27 kcal mol^{-1} from the experimental value.

4.2. Three-Body Energy Terms. *4.2.1. Three-Body Dynamical Correlation Energy.* The three-body dynamical correlation energy assumes the usual form of a summation in inverse powers of the fragment separation distances:[36]

$$V_{dc}^{(3)} = -\sum_{i=1}^{3}\sum_{n} f_i(\mathbf{R})\chi_n(r_i)C_n^{(i)}(R_i, \theta_i)r_i^{-n} \quad (10)$$

where the first summation includes all atom−diatom interactions ($i \equiv A - BC$). R_i is the diatomic internuclear distance, r_i is the separation between atom A and the center-of-mass of the BC diatomic coordinate, and θ_i is the angle between the two associated vectors (see Figure 1 of ref 37). $f_i = 1/2\{1 - \tanh[\xi(\eta R_i - R_j - R_k)]\}$ is a convenient switching function, where we have fixed $\eta = 6$ and $\xi = 0.6a_0^{-1}$; corresponding expressions apply to R_j, R_k, f_j, and f_k. In turn, $\chi_n(r_i)$ is a damping function, which also assumes the form of eq 7, but with R replaced by the center-of-mass separation for the relevant atom−diatom channel. In addition, the atom−diatom dispersion coefficients in eq 10 are

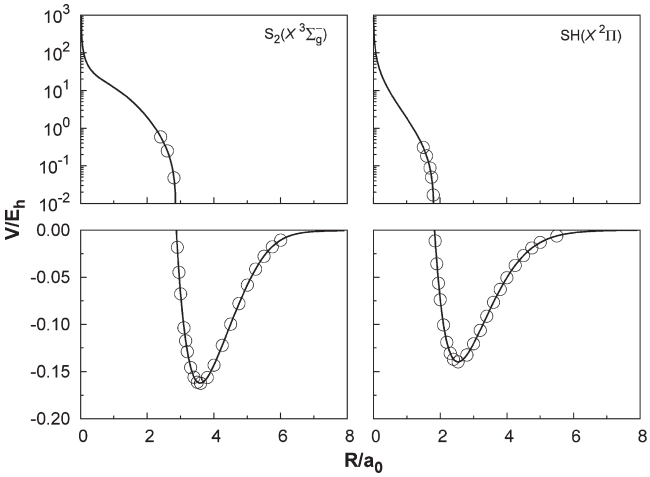

Figure 1. EHFACE2U potential energy curves for $SH(X^2\Pi)$ and $S_2(X^3\Sigma_g^-)$. The ○ indicate the ab initio energies extrapolated to CBS limit and the lines the EHFACE2U curves.

Table 1. Equilibrium Geometries (bohr), Vibrational Frequencies (cm^{-1}), and Dissociation Energies (kcal mol^{-1}) for SH and S_2

	$SH(X^2\Pi)$				$S_2(X^3\Sigma_g^-)$				
	R_e	ω_e	D_0	D_e	R_e	ω_e	D_0	D_e	ΔE^a
MRCI(Q)/AVDdZ[b]	2.5615	2676.4	77.43	81.26	3.6465	689.8	85.60	86.59	5.33
MRCI(Q)/AV*T*dZ[b]	2.5380	2687.8	81.67	85.51	3.6106	707.7	94.47	95.46	9.95
MRCI(Q)/AVQdZ[b]	2.5361	2694.4	83.03	86.88	3.5937	719.8	98.29	99.32	12.44
MRCI(Q)/AV5dZ[b]	2.5351	2694.1	83.42	87.27	3.5881	722.4	100.21	101.24	13.97
DMBE/CBS PES[c]	2.5354	2697.5	83.91	87.77	3.5841	731.0	100.90	101.95	14.18
CCSD(T)/AV*T*dZ[d]	2.5388	2688.6	81.49	85.33	3.6022	714.4	94.26	95.28	9.95
CCSD(T)/AVQdZ[d]	2.5371	2696.3	82.79	86.64	3.5850	726.1	98.29	99.33	12.69
CCSD(T)/AV5dZ[d]	2.5362	2696.7	83.19	87.05	3.5793	728.7	99.86	100.90	13.85
CBS[d]	2.5358	2697.7	83.58	87.44	3.5742	731.5	101.34	102.39	14.95
CBS+CV[d]	2.5328	2701.2	83.70	87.56	3.5669	734.2	101.67	102.72	15.16
CBS+CV+T[d]	2.5336	2696.9	83.75	87.61	3.5672	734.4	101.44	102.49	14.88
CBS+T/TZ [d]	2.5334	2697.6	83.70	87.56	3.5667	735.1	101.05	102.10	14.54
CBS [e]					3.5733	723.3			
expt.[f]	2.5339	2695.8	83.50 ± 0.7	87.35 ± 0.7	3.5701	725.7	100.76 ± 0.02	101.80 ± 0.02	14.45 ± 0.72
expt.[g]								101.89 ± 0.007	

[a] $\Delta E = D_e(S_2) - D_e(SH)$. [b] This work. Obtained from potential energy curves fitted to MRCI(Q)/AV*X*dZ($X = D,T,Q,5$) energies. [c] This work. Obtained from DMBE/CBS PES. [d] Reference 13, the dissociation energies are calculated by $D_e = D_0 + \omega_e/2$. [e] Reference 59, the CBS value of $R_e(S_2)$ is calculated using the CCSDT/AV(*Q*,5)dZ energies, while $\omega_e(S_2)$ is calculated using the CCSD(T)/AV(*D*,*T*)dZ energies. [f] References 56, 60. [g] Reference 61.

defined by

$$C_n^{(i)} = \sum_L C_n^L P_L(\cos\theta_i) \quad (11)$$

where $P_L(\cos\theta_i)$ denotes the Lth term of the Legendre polynomial expansion and C_n^L are the associated expansion coefficients. The expansion in eq 11 has been truncated by considering only the coefficients C_6^0, C_6^2, C_8^0, C_8^2, C_8^4, and C_{10}^0; all other coefficients have been assumed to make a negligible contribution, and are hence neglected. This approximation may be well justified for closed shell atom-homonuclear interactions, but, given other approximations (see later), we assume it as a valid one throughout. To estimate the dispersion coefficients, we have utilized the generalized Slater−Kirkwood approximation.[38] As usual, the atom−diatom dispersion coefficients so calculated for a set of internuclear distances have then been fitted to the form:

$$C_n^{L,\mathrm{A-BC}}(R) = C_n^{L,\mathrm{AB}} + C_n^{L,\mathrm{AC}} + D_\mathrm{M}\left(1 + \sum_{i=1}^{3} a_i r^i\right)\exp\left(-\sum_{i=1}^{3} b_i r^i\right) \quad (12)$$

where $r = R - R_\mathrm{M}$ is the displacement relative to the position of the maximum and $b_1 = a_1$. $C_n^{L,\mathrm{AB}}$, for $L = 0$, are the corresponding atom−atom dispersion coefficients (for $L \neq 0, C_n^{L,\mathrm{AB}} = 0$). The least-squares parameters that result from such fits are collected in Table 2 of the Supporting Information, while their internuclear dependences are displayed in Figure 1 of the Supporting Information. Note that, for $R = 0$, the isotropic component of the dispersion coefficient is fixed at the corresponding value in the A−X pair, where X represents the united atom of BC at the limit of a vanishingly small internuclear separation. As pointed out elsewhere,[36] eq 10 causes an overestimation of the dynamical correlation energy at the atom−diatom dissociation channel. To correct such a behavior, we have multiplied the two-body dynamical correlation energy for the i-pair by $\Pi_{j\neq i}(1 - f_j)$, correspondingly for channels j and k. This ensures that the only two-body contribution at the ith channel is that of BC.

4.2.2. Three-Body Electrostatic Energy. Because the H atom has spherical symmetry, the long-range electrostatic potential terms of HS_2 only arise from the interaction of the permanent quadrupole moment of the sulfur atom with the permanent dipole and quadruple moments of SH diatom. Following previous work,[39−41] the electrostatic energy is written as

$$V_\mathrm{ele}^{(3)} = f(\mathbf{R})\{C_4(R,r)A_{DQ}(\theta_\mathrm{a},\theta,\phi_\mathrm{ab}))r^{-4} + C_5(R,r)A_{QQ}(\theta_\mathrm{a},\theta,\phi_\mathrm{ab}))r^{-5}\} \quad (13)$$

where the $f(\mathbf{R})$, R, r, and θ have the same meaning as in section 4.2.1, the θ_a is the angle that defines the atomic quadrupole orientation, and ϕ_ab is the corresponding dihedral angle. The coefficients $C_4(R,r)$ and $C_5(R,r)$ are given by

$$\begin{aligned} C_4(R,r) &= \frac{3}{2} Q_\mathrm{S} D_\mathrm{SH}(R)\chi_4(r) \\ C_5(R,r) &= \frac{3}{4} Q_\mathrm{S} Q_\mathrm{SH}(R)\chi_5(r) \end{aligned} \quad (14)$$

where the $D_\mathrm{SH}(R)$ and $Q_\mathrm{SH}(R)$ are the permanent electric dipole and quadruple moments of SH, and Q_S is the quadruple moment of the sulfur atom. The functional form of the angular variations of A_{DQ} and A_{QQ} take the expressions employed in previous work[39,41,42] based on the classical-optimized-quadruple (COQ) model.[43−47]

Table 2. Numerical Values, for SH Dipole and Quadrupole Moments

quantity	D_SH	Q_SH
Q_∞/ea_0^2		1.014
M_6/ea_0^8		20 000
R_ref/a_0	2.2198	3.7669
D_M^a	0.308922	0.716170
a_1/a_0^{-1}	−0.090708	0.088913
a_2/a_0^{-2}	−0.158775	−0.337353
a_3/a_0^{-3}	0.038302	0.266863
b_1/a_0^{-1}	−0.090708	−0.208205
b_2/a_0^{-2}	−0.064710	0.508490
b_3/a_0^{-3}	0.062764	0.112271

[a] The units are in ea_0 for D_SH and ea_0^2 for Q_SH.

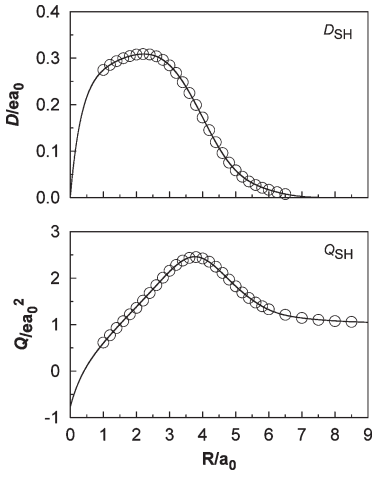

Figure 2. Variation of SH dipole and quadrupole moments with internuclear distance.

The analytical expression for the SH dipole has been obtained by fitting our own ab initio results to the form:[48]

$$D(R) = D_\mathrm{M}(1 + \sum_{i=1}^{3} a_i r^i)\exp(-\sum_{i=1}^{3} b_i r^i) \quad (15)$$

where $r = R - R_\mathrm{ref}$ and R_ref is the reference distance corresponding to the maximum in the $D(R)$ curve, and $b_1 \equiv a_1$. In turn, the variation of the SH quadrupole moment with the internuclear distance has been fitted to the following model:[47]

$$Q(R) = D_\mathrm{M}(1 + \sum_{i=1}^{3} a_i r^i)\exp(-\sum_{i=1}^{3} b_i r^i) + Q_\infty + \chi_8(R)\frac{M^6}{R^6} \quad (16)$$

where $r = R - R_\mathrm{ref}$, with R_ref being the reference distance corresponding to the maximum in the $Q(R)$ curve. Q_∞ is the value of the separated-atoms quadrupole limit. The parameters in eqs 15 and 16 are collected in Table 2, while their graphical view of the modeled functions can be seen in Figure 2.

4.2.3. Three-Body Extended Hartree−Fock Energy. By removing, for a given triatomic geometry, the sum of the two-body energy terms from the corresponding DMBE interaction energies eq 5, which was defined with respect to the infinitely separated

dx.doi.org/10.1021/jp201980m |J. Phys. Chem. A 2011, 115, 5274–5283

ground-state atoms, one obtains the total three-body energy. Next, by subtracting the three-body dynamical correlation contribution eq 10 and the three-body electrostatic energy eq 13 from the total three-body energy, one obtains the three-body extended Hartree–Fock energy. This can be represented by the following three-body distributed-polynomial[41] form:

$$V_{\mathrm{EHF}}^{(3)} = \sum_{j=1}^{3} P^{j}(Q_1, Q_2, Q_3) \times \prod_{i=1}^{3}\{1 - \tanh[\gamma_i^j(R_i - R_i^{j,\mathrm{ref}})]\} \qquad (17)$$

where $P^j(Q_1,Q_2,Q_3)$ is the jth polynomial up to six-order in the symmetry coordinates. As usual, we obtain the reference geometries $R_i^{j,\mathrm{ref}}$ by first assuming their values to coincide with bond distances of the associated stationary points. Subsequently, we relax this condition via a trial-and-error least-squares fitting procedure. Similarly, the nonlinear range-determining parameters γ_i^j have been optimized in this way. The complete set of parameters amounts to a total of 150 linear coefficients c_i, 9 nonlinear coefficients γ_i^j, and 9 reference geometries $R_i^{j,\mathrm{ref}}$. All of the numerical values of the least-squares parameters are gathered in Tables 3 and 4 of the Supporting Information. Table 3 shows the partial and accumulated stratified root-mean-squared deviations (rmsd) of the final DMBE/CBS PES with respect to all the fitted ab initio energies. As shown in Table 3, a total of 1601 points have been used for the calibration procedure, with the energies covering a range up to 1000 kcal mol^{-1} above the HS_2 global minimum. The fit shows that the total root-mean-square derivation is 0.853 kcal mol^{-1}.

5. FEATURES OF THE POTENTIAL ENERGY SURFACE

Table 4 gathers the relative energies of the present DMBE/CBS PES. The results carried out by Peterson et al.[13] at the CCSD(T)/AV*X*dZ level and those by Francisco[12] at the CCSD(T)/AV*X*Z level are also gathered in this table for comparison. The energies of H + S_2 relative to the $HS_2(X^2A'')$ global minimum calculated by Francisco at CCSD(T)/AV*X*Z (X = T,Q,5) are 55.1, 55.8, and 55.9 kcal mol^{-1}, with the CBS limit having a value of 56.2 kcal mol^{-1}, thus ∼4.9 kcal mol^{-1} smaller than the CCSD(T)/AV*X*dZ (X = T,Q,5) values reported by Peterson et al.[13] For the relative energies of S + SH, Francisco[12] predicts values ∼2.0 kcal mol^{-1} smaller than those of Peterson et al.[13] This suggests that one needs to include the core-polarization high-exponent d functions (AV*X*dZ) as recommended[49,50] for compounds containing second-row atoms, such as the title one. The relative energies for H + S_2 and S + SH calculated from the present DMBE/CBS PES, which are extrapolated to CBS utilizing the MRCI(Q)/AV(T,Q)dZ scheme described above, are predicted to be 60.95 and 75.13 kcal mol^{-1}, showing differences of 0.07 and 0.77 kcal mol^{-1} relative to the values of Peterson et al.,[13] respectively. In turn, the well depth of the HS_2 global minimum predicted from our DMBE/CBS PES is 162.90 kcal mol^{-1}, which agrees well with the CBS result (163.27 kcal mol^{-1}) by Peterson et al.[13] Indeed, the difference is only 0.37 kcal mol^{-1} despite the fact that smaller basis sets have here been utilized. The calculated hydrogen atom exchange barrier for the HSS → SSH reaction is 33.63 kcal mol^{-1}, which is ∼1.93 kcal mol^{-1} lower than the CBS result (31.7 ± 1.0 kcal mol^{-1}) suggested by Francisco.[12]

Table 5 compares the attributes of the stationary points (geometry, energy, and vibrational frequencies) of the HS_2 DMBE/CBS PES with the other theoretical and experimental results. The global minimum for the HS_2 ground state from our DMBE/CBS PES is predicted to be located at R_{SS} = 3.7106a_0, R_{SH} = 2.5306a_0, and ∠HŜS = 101.96°, and the result from our fit to dense grid CBS/MRCI(Q)/AV(T,Q)dZ points gives that R_1 = 3.7072a_0, R_2 = 2.5439a_0, and ∠HSS = 102.37°, thus differing by 0.0034a_0, 0.0133a_0, and 0.41°. The results calculated by Peterson et al., which are extrapolated to CBS limit using CCSD(T)/AV(Q,5)dZ energies, are R_1 = 3.7099a_0, R_2 = 2.5509a_0, and ∠HSS = 101.50°, and the corresponding experimental[51] values are R_{SS} = 3.7044a_0, R_{SH} = 2.5555a_0, and ∠HSS = 101.74°, with the differences from the result of our DMBE/CBS PES being (0.0007a_0,0.0203a_0,0.46°) and (0.0064a_0,0.0249a_0,0.22°) in the above order. As for the harmonic frequencies, the DMBE/CBS PES from the present work predicts values of 588, 873, and 2597 cm^{-1} (SS stretch, HSS bending, and SH stretch, respectively), with the results from the fit to the calculated dense grid of points being 552, 909, and 2488 cm^{-1}. The most recent experimental values given by Ashworth et al.[8] are 596, 892, and 2688 cm^{-1}. The corresponding results reported by Peterson et al.,[13] who have extrapolated to CBS using CCSD(T)/AV(Q,5)dZ energies, are 607, 919, and 2600 cm^{-1}. Clearly, the differences from that of our DMBE/CBS PES are quite small, amounting to (19, 47, 3) cm^{-1} in the above order. As seen in Table 5, the results from our DMBE/CBS PES are also in good agreement with other available experimental and theoretical values.

Figures 3–8 illustrate the main topographical features of the HS_2 DMBE/CBS PES. Figure 3 shows energy contours for SS and SH stretching with the HSS angle kept fixed at the corresponding equilibrium value, while Figure 4 shows contours for the SS and SH stretching at the S–S–H collinear configuration. In turn, Figure 5 shows a contour plot for the stretching of the

Table 3. Accumulated (acc) and Stratum (strat) Root-Mean-Square Deviations (kcal mol^{-1}) of the DMBE Potential Energy Surface

energy		N^a		max. dev^b		rmsd		$N_{>\mathrm{rmsd}}{}^c$	
acc	strat	acc	strat	acc	strat	acc	strat	acc	strat
10	0–10	51	51	0.288	0.288	0.120	0.120	15	15
20	10–20	95	44	0.677	0.677	0.231	0.313	28	15
30	20–30	151	56	0.915	0.915	0.332	0.455	47	23
40	30–40	263	112	2.284	2.284	0.462	0.594	67	31
50	40–50	350	87	2.284	2.027	0.548	0.750	97	24
60	50–60	448	98	2.918	2.918	0.587	0.709	121	30
70	60–70	618	170	3.425	3.425	0.586	0.584	154	33
80	70–80	795	177	3.425	3.270	0.577	0.541	190	40
90	80–90	917	122	3.425	3.058	0.599	0.731	225	37
100	90–100	1011	94	3.425	3.128	0.617	0.766	253	27
150	100–150	1388	377	3.671	3.671	0.651	0.734	318	73
200	150–200	1451	63	3.848	3.848	0.712	1.529	325	23
250	200–250	1488	37	3.848	3.742	0.745	1.570	329	12
500	250–500	1591	103	4.419	4.419	0.851	1.777	315	31
1000	500–1000	1601	10	4.419	1.926	0.853	1.151	322	5

[a] Number of calculated DMBE/CBS points up to the indicated energy range. [b] Maximum deviation up to the indicated energy range. [c] Number of calculated DMBE/CBS points with an energy deviation larger than the rmsd.

two SH bonds at a S−H−S linear configuration. The notable features from Figure 5 are the two equivalent asymmetric hydrogen-bonded minima, which are separated by a barrier lying halfway between them. The location of the barrier is found to be $R_{SS} = 5.8752a_0$ and $R_{SH} = 2.9376a_0$, with the harmonic frequencies at the top being 250, 690i, and 1750i cm^{-1}, respectively.

Figure 6 shows a contour plot for the C_{2v} insertion of H into the S_2 diatomic. The important features from this figure are the saddle point structure for the HSS → SSH isomerization (see text before) and the barrier for the H + S_2 reaction. The saddle point for isomerization is found to be located at $R_{SS} = 3.9047a_0$, $R_{SH} = 2.9398a_0$, and $\angle H\hat{S}S = 48.39°$, with the barrier height lying at −0.2060 E_h, and the harmonic frequencies being 1577i, 562, and 1886 cm^{-1}. As compared to the results of Francisco,[12] the agreement is good. The barrier is located at $R_{SS} = 3.6146a_0$ and $R_{SH} = 4.2960a_0$, with the well depth being −0.1500 E_h. The vibrational frequencies are also gathered in Table 5.

Figure 7 shows a contour plot for a H atom moving around a SS diatom with the bond length fixed at $R_{SS} = 3.5841a_0$, which lies along the *X*-axis with the center of the bond fixed at the origin. The two salient features are the deep minima connected by a C_{2v} saddle point, which allows scrambling of the two surfur atoms. Also visible along the C_{2v} line is a closed contour apparently showing a maximum. It is indeed a conical intersection that is undescribable within the present single-sheeted DMBE formalism. In turn, Figure 8 shows a contour plot for S atom moving around a fixed SH diatom with the bond length fixed at $R_{SH} = 2.5354a_0$, which lies along the *X*-axis with the center of the bond fixed at the origin. The two plots clearly reveal a smooth behavior both at short- and at long-range regions.

Shown in Figures 9 and 10 are the spherically averaged isotropic (V_0) and leading anisotropic potentials for H + S_2(V_2) and S + SH(V_1,V_2) scattering processes with the diatoms fixed at their equilibrium geometries. Note that the magnitude of the isotropic average potential V_0 determines how close on average the atom and molecule can approach each other, while the sign of V_2 indicates whether or not the molecule prefers to orient its axis along the direction of the incoming atom: a negative value favors the collinear approach, while a positive value favors the approach through an isosceles triangular geometry. For the S−SH interaction, there is a balance that makes a prediction not so readily done. Specifically, it is shown in Figure 10 that there is no barrier in the spherically averaged isotropic term (V_0), while the

Table 4. Relative Energetics for HS_2 DMBE/CBS PES

	relative energetics[a]			
level of theory	D_e(H + S_2)	D_e (S + SH)	D_e (H + 2S)	D_e([HSS → SSH]‡)
DMBE/CBS PES[b]	60.95	75.13	162.90	33.63
CCSD(T)/AV*T*dZ[c]	60.01	69.97	155.30	
CCSD(T)/AVQdZ[c]	60.63	73.31	159.96	
CCSD(T)/AV5dZ[c]	60.77	74.63	161.67	
CBS[c]	60.88	75.90	163.27	
CBS+CV[c]	60.71	76.07	163.61	
CBS+CV+T[c]	61.16	76.04	163.65	
CCSD(T)/AV*TZ*[d]	55.1	67.4		30.5
CCSD(T)/AV*QZ*[d]	55.8	71.3		31.2
CCSD(T)/AV5Z[d]	55.9	73.5		31.6
CBS[d]	56.2	74.1		31.7 ± 1

[a] The unit of energy is kcal mol^{-1}. [b] This work. [c] Reference 13. [d] Reference 12.

Table 5. Comparison of Stationary Points of HS_2 DMBE/CBS PES[a]

	R_{SS}/a_0	R_{SH}/a_0	$\angle H\hat{S}S$/o	E/E_h	ω_1(S−S)	ω_2(bend)	ω_3(S−H)
			Global Minimum				
ab initio[b]	3.7072	2.5439	102.37	−0.2596	552	909	2488
DMBE/CBS PES[c]	3.7106	2.5306	101.96	−0.2596	588	873	2597
exp.	3.7044[d]	2.5555[d]	101.74[d]		596,[f] 595,[g] 600[h]	934,[e] 892,[f] 904[g]	2463,[e] 2688[f]
CCSD(T)/cc-pV*T*dZ[i]	3.7426	2.5489	101.40		592	913	2607
B3LYP/6-311+G(3df,2p)[i]	3.7356	2.5610	102.13		586	910	2556
CCSD(T)/AV*TZ*[j]	3.7662	2.5549	100.90		585	904	2607
CCSD(T)/AV*QZ*[j]	3.7360	2.5530	101.30		598	910	2604
CCSD(T)/AV5Z[j]	3.7190	2.5511	101.40				
CBS[k]	3.7099	2.5509	101.50		607	919	2600
			HS_2 Isomerization				
ab initio[b]	3.9091	2.9372	48.12	−0.2061	1345i	548	1935
DMBE/CBS PES[c]	3.9047	2.9398	48.39	−0.2060	1577i	562	1886
CCSD(T)/AV*TZ*[j]	3.9533	2.9347	47.70		1208i	538	1919
CCSD(T)/AV*QZ*[j]	3.9231	2.9310	48.00		1275i	548	1933
CCSD(T)/AV5Z[j]	3.9042	2.9291	48.20				
			T-Shaped H−S_2 Structure				
DMBE/CBS PES[c]	3.6146	4.2960	65.12	−0.1500	700	994i	1074i
			S−H−S Saddle Point				
DMBE/CBS PES[c]	5.8752	2.9376	0	−0.1165	250	690i	1750i

[a] Harmonic frequencies are in cm^{-1}. [b] From a polynomial fit to a dense grid of extrapolated CBS/MRCI(Q)/AV(*T*,Q)dZ points. [c] This work. [d] Experiment values.[51] [e] Experiment values.[7] [f] Experiment values.[8] [g] Experiment values.[62] [h] Experiment values.[63] [i] Reference 11. [j] Reference 12. [k] Reference 13. The CBS limit was obtained by extrapolation of the AVQdZ and AV5dZ CCSD(T) correlation energies.

dx.doi.org/10.1021/jp201980m |*J. Phys. Chem. A* 2011, 115, 5274–5283

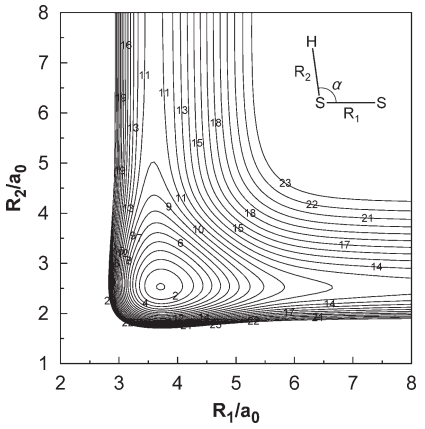

Figure 3. Contour plot for bond stretching in H−S−S, keeping the HSS angle fixed at 101.96°. Contours are equally spaced by 0.01 E_h, starting at −0.259 E_h.

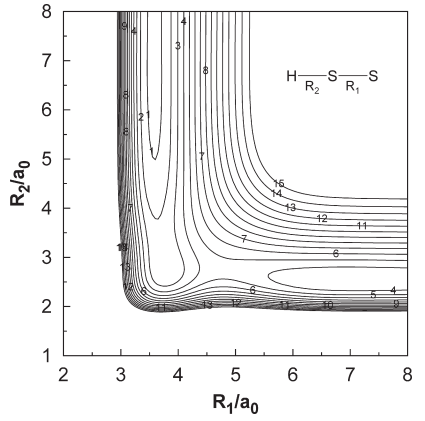

Figure 4. Contour plot for bond stretching in S−S−H collinear configuration. Contours are equally spaced by 0.0085 E_h, starting at −0.16 E_h.

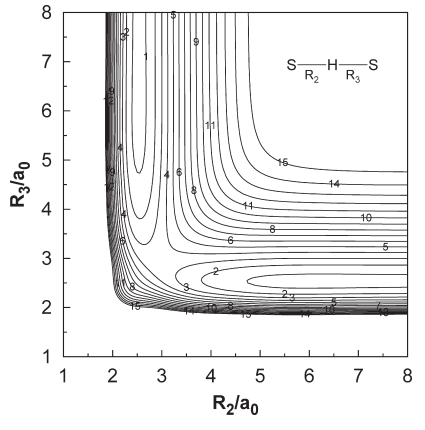

Figure 5. Contour plot for bond stretching in linear S−H−S. Contours are equally spaced by 0.0085 E_h, starting at −0.138 E_h.

anisotropic (V_2) component is non-negative at the regions of interest. This is partly compensated with a strongly attractive V_1 contribution from intermediate up to long-range interaction regimes. From their balance and the fact that the reaction is exoergic,

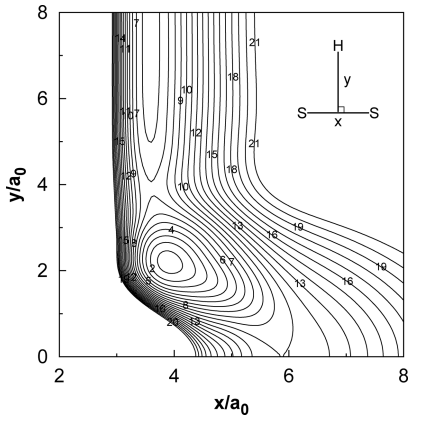

Figure 6. Contour plot for C_{2v} insertion of H atom into S_2 diatom. Contours are equally spaced by 0.0085 E_h, starting at −0.21 E_h.

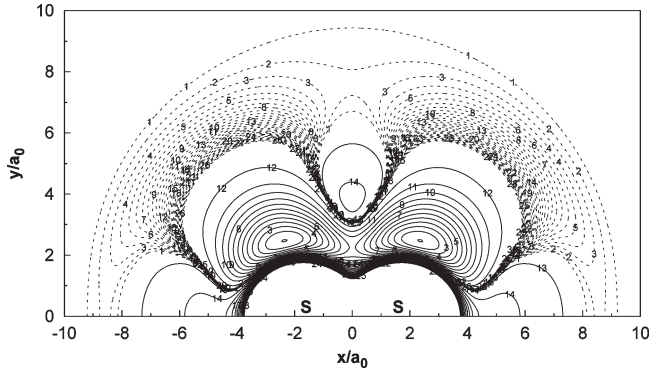

Figure 7. Contour plot for a H atom moving around a SS diatom with bond length fixed at $R_{SS} = 3.5841a_0$ (this lies along the X-axis with the center of the bond fixed at the origin). Contours are equally spaced by 0.009 E_h, starting at −0.258 E_h. The dashed lines are contours equally spaced by −0.00008 E_h, starting at −0.1625 E_h.

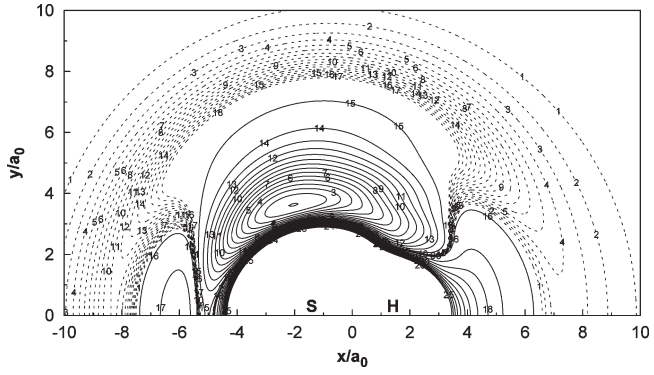

Figure 8. Contour plot for a S atom moving around a SH diatom with bond length fixed at $R_{SH} = 2.5354a_0$ (this lies along the X-axis with the center of the bond fixed at the origin). Contours are equally spaced by 0.008 E_h, starting at −0.2594 E_h. The dashed lines are contours equally spaced by −0.0002 E_h, starting at −0.1402 E_h.

it turns out that the S + SH reaction occurs much easier than the H + S_2 reverse reaction. The present result therefore supports that of Mihelcic and Schindler,[52] who have shown the reaction of SH radicals with S atom to form S_2 and H to occur with a fast rate.

dx.doi.org/10.1021/jp201980m |J. Phys. Chem. A 2011, 115, 5274–5283

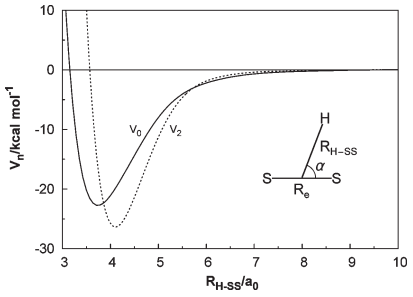

Figure 9. Isotropic (V_0) and leading anisotropic (V_2) components of H−SS interaction potential energy, with the diatom fixed at its equilibrium geometry.

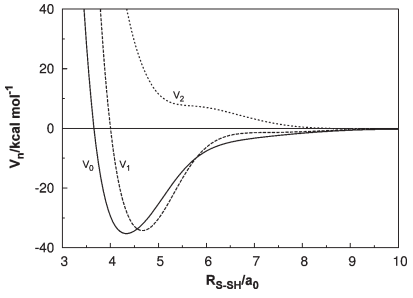

Figure 10. Isotropic (V_0) and leading anisotropic (V_1,V_2) components of S−SH interaction potential energy, with the diatom fixed at its equilibrium geometry.

In fact, the experimental findings of Porter[5] also support that the origin of the HS_2 radical stems from the reaction of an S atom with a SH radical. Indeed, the recent theoretical calculations by Francisco[12] also seem to support the same conclusion.

Finally, preliminary rate constant calculations have been carried out for the reaction S + SH → H + S_2 by running quasi-classical trajectories (QCT) on the PES of the present work at two temperatures, 298 and 400 K. A total of 5000 trajectories per temperature has been employed, with an integration step size chosen to be 1.5×10^{-16} s such as to warrant conservation of the total energy to better than one part in 10^3. The trajectories have been started at a distance between the incoming atom and the center-of-mass of the diatom of 9 Å, a value considered sufficiently large to make the interaction energy negligible.

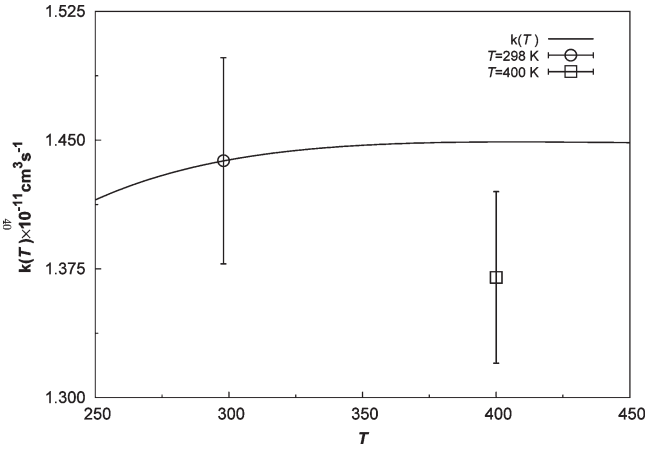

Figure 11. Temperature dependence of the rate constant as predicted by eq 18 for the reaction S + SH → H + S_2. Also shown by the symbols are the QCT results actually calculated at T = 298 K and T = 400 K, jointly with the associated error bars.

Table 6. Rate Constant (in 10^{-11} cm^3 s^{-1}) at 298 K for S + SH Reaction

	T/K	$k(T)$
DMBE/CBS PES	298	1.44 ± 0.06[a]
exp.	295	<0.498[b]
	295	4.0[c]
	300	4.5[d]

[a] This work. [b] Reference 59. [c] Reference 57. [d] Reference 52.

The thermal rate constant for the formation of S + SH assumes the general form:

$$k(T) = g_e(T)\left(\frac{8k_BT}{\pi\mu_{S+SH}}\right)^{1/2}\frac{N_r}{N}\pi b_{max}^2 \qquad (18)$$

with the estimated error of the rate constant being given by $\Delta k(T) = k(T)[(N - N_r)/NN_r]^{1/2}$; T is the temperature, k_B is the Boltzmann constant, b_{max} is the maximum impact parameter, N_r is the number of reactive trajectories in a total of N, μ_{S+SH} is the reduced mass of the reactants, and $g_e(T)$ is the electronic degeneracy factor,[53,54] which assumes the form:

$$g_e(T) = \frac{2}{[5 + 3\exp(-569.83/T) + \exp(-825.34/T)] \times [2 + 2\exp(-542.36/T)]} \qquad (19)$$

where 2 in the numerator is the degeneracy of the $HS_2(X^2A'')$ PES, and the denominator corresponds to the electronic partition function of the reagents: the first part is the electronic degeneracy of S(^{3}P), which splits into $^3P_2$, $^3P_1$, and $^3P_0$ with the energy gaps[55] 569.83 and 825.34 K; the second part is the degeneracy of SH($^2\Pi$) with the two (Π) levels split into $^2\Pi_{1/2} - {}^2\Pi_{3/2}$, which has an energy gap[56] of 542.36 K, and 2 is here because each of these two states is doubly degenerate.

The result at T = 298 K is compared to the available experimental data in Table 6. The thermalized rate constant is predicted to be $(1.44 \pm 0.06) \times 10^{-11}$ cm^3 s^{-1}, thus about 2−3 times smaller than two of the reported experimental values: 4.0×10^{-11}[57] and 4.5×10^{-11} cm^3 s^{-1}.[52] In turn, the experimental result of 0.498×10^{-11} cm^3 s^{-1} by Nicholas et al.[58] underestimates our prediction by about a factor similar to that above. The temperature dependence of the rate constant predicted by eq 18 is depicted in Figure 11. Also shown are the actually calculated QCT results at T = 298 and 400 K, as well as the associated error bars. Not surprisingly, the rate constant value of 1.45×10^{-11} cm^3 s^{-1} predicted by eq 18 at T = 400 K slightly overestimates our test calculation of

dx.doi.org/10.1021/jp201980m |J. Phys. Chem. A 2011, 115, 5274–5283

$(1.37 \pm 0.05) \times 10^{-11}$ cm^3 s^{-1} at 400 K, because the former is based on the average velocity for 298 K. In fact, a decreasing trend with temperature of the rate constant is to be expected because the title reaction occurs on a barrier-free PES. A full detailed analysis of the dynamics and kinetics will be reported elsewhere.

6. CONCLUDING REMARKS

We have reported a global DMBE/CBS PES for the electronic ground state of HS_2, on the basis of fitting ab initio energies extrapolated to CBS limit. The USTE(T,Q) extrapolation scheme is employed to warrant CBS-limit accuracy even though the calculations employed relatively inexpensive basis sets. As shown above, the DMBE/CBS PES describes all major topographical features of the HS_2 PES except those forbidden within the employed single-sheeted approach. Indeed, a comparison of its attributes with experimental and other accurate theoretical values shows quite a good agreement. This and the results of preliminary rate constant calculations clearly commend the use of the current PES for more detailed adiabatic dynamics studies of the title reaction.

■ ASSOCIATED CONTENT

Supporting Information. Tables of parameters in the two-body energy curves, numerical values of the parameters in eqs 12 and 17, and plots of dispersion coefficients for the atom−diatom channels. This material is available free of charge via the Internet at http://pubs.acs.org.

■ AUTHOR INFORMATION

Corresponding Author
*E-mail: varandas@qtvs1.qui.uc.pt.

■ ACKNOWLEDGMENT

This work has the support of Fundação para a Ciência e a Tecnologia, Portugal.

■ REFERENCES

(1) Glavas, S.; Toby, S. *J. Phys. Chem.* **1975**, *79*, 779.
(2) Slagle, I. R.; Graham, R. E.; Gutman, D. *Int. J. Chem. Kinet.* **1976**, *8*, 451.
(3) Gargurevich, I. A. *Ind. Eng. Chem. Res.* **2005**, *44*, 7706.
(4) Sendt, K.; Jazbec, M.; Haynes, B. S. *Proc. Combust. Inst.* **2002**, *29*, 2439.
(5) Porter, G. *Discuss. Faraday Soc.* **1950**, *9*, 60.
(6) Yamamoto, S.; Saito, S. *Can. J. Phys.* **1994**, *72*, 954.
(7) Isoniemi, E.; Khriachtchev, L.; Pettersson, M.; Räsänen, M. *Chem. Phys. Lett.* **1999**, *311*, 47.
(8) Ashworth, S. H.; Fink, E. H. *Mol. Phys.* **2007**, *105*, 715.
(9) Sannigrahi, A. B.; Peyerimhoff, S. D.; Buenker, R. J. *Chem. Phys. Lett.* **1977**, *46*, 415.
(10) Owens, Z. T.; Larkin, J. D.; Schaefer, H. F., III. *J. Chem. Phys.* **2006**, *125*, 164322.
(11) Denis, P. A. *Chem. Phys. Lett.* **2006**, *422*, 434.
(12) Francisco, J. S. *J. Chem. Phys.* **2007**, *126*, 214301.
(13) Peterson, K. A.; Mitrushchenkov, A.; Francisco, J. S. *Chem. Phys.* **2008**, *346*, 34.
(14) Varandas, A. J. C. *Conical Intersections: Electronic Structure, Spectroscopy and Dynamics*; World Scientific Publishing: River Edge, NJ, 2004; Chapter 5, p 91, Advanced Series in Physical Chemistry.
(15) Varandas, A. J. C. *Adv. Chem. Phys.* **1988**, *74*, 255.
(16) Varandas, A. J. C. In *Lecture Notes in Chemistry*; Laganá, A., Riganelli, A., Eds.; Springer: Berlin, 2000; Vol. 75, pp 33−56.
(17) Varandas, A. J. C. *J. Mol. Struct. (THEOCHEM)* **1985**, *120*, 401.
(18) Werner, H.-J.; Knowles, P. J. *J. Chem. Phys.* **1988**, *89*, 5803.
(19) Werner, H.-J.; Knowles, P. J. *Chem. Phys. Lett.* **1988**, *145*, 514.
(20) Langhoff, S. R.; Davidson, E. R. *Int. J. Quantum Chem.* **1974**, *8*, 61.
(21) Knowles, P. J.; Werner, H.-J. *Chem. Phys. Lett.* **1985**, *115*, 259.
(22) Werner, H.-J.; Knowles, P. J.; Lindh, R.; Schütz, M.; Celani, P.; Korona, T.; Manby, F. R.; Rauhut, G.; Amos, R. D.; Bernhardsson, A.; Berning, A.; Cooper, D. L.; Deegan, M. J. O.; Dobbyn, A. J.; Eckert, F.; Hampel, C.; Hetzer, G.; Lloyd, A. W.; McNicholas, S. J.; Meyer, W.; Mura, M. E.; Nicklass, A.; Palmieri, P.; Pitzer, R.; Schumann, U.; Stoll, H.; Stone, A. J.; Tarroni, R.; Thorsteinsson, T. *MOLPRO, version 2002.6, a package of ab initio programs*, 2003; see http://www.molpro.net.
(23) Dunning, T. H., Jr. *J. Chem. Phys.* **1989**, *90*, 1007.
(24) Kendall, R. A.; Dunning, T. H., Jr.; Harrison, R. J. *J. Chem. Phys.* **1992**, *96*, 6769.
(25) Basis sets were obtained from the Extensible Computational Chemistry Environment Basis Set Database, Version 01/15/07, as developed and distributed by the Molecular Science Computing Facility, Environmental and Molecular Sciences Laboratory, which is part of the Pacific Northwest Laboratory, P.O. Box 999, Richland, WA 99352, and funded by the U.S. Department of Energy. The Pacific Northwest Laboratory is a multiprogram laboratory operated by Battelle Memorial Institute for the U.S. Department of Energy under contract DE-AC06-76RLO 1830. Contact Karen Schuchardt for further information.
(26) Varandas, A. J. C. *J. Chem. Phys.* **2007**, *126*, 244105.
(27) Karton, A.; Martin, J. M. L. *Theor. Chem. Acc.* **2006**, *115*, 330.
(28) Varandas, A. J. C. *J. Chem. Phys.* **2000**, *113*, 8880.
(29) Song, Y. Z.; Varandas, A. J. C. *J. Chem. Phys.* **2009**, *130*, 134317.
(30) Li, Y. Q.; Varandas, A. J. C. *J. Phys. Chem. A* **2010**, *114*, 9644.
(31) Galvão, B. R. L.; Rodrigues, S. P. J.; Varandas, A. J. C. *J. Chem. Phys.* **2008**, *129*, 044302.
(32) Galvão, B. R. L.; Varandas, A. J. C. *J. Phys. Chem. A* **2009**, *113*, 14424.
(33) Varandas, A. J. C. *J. Phys. Chem. A* **2010**, *114*, 8505.
(34) Varandas, A. J. C.; Silva, J. D. *J. Chem. Soc., Faraday Trans.* **1992**, *88*, 941.
(35) Le Roy, R. J. *Spec. Period. Rep. Chem. Soc. Mol. Spectrosc.* **1973**, *1*, 113.
(36) Varandas, A. J. C. *J. Chem. Phys.* **1996**, *105*, 3524.
(37) Varandas, A. J. C. *Chem. Phys. Lett.* **1992**, *194*, 333.
(38) Matías, M. A.; Varandas, A. J. C. *Mol. Phys.* **1990**, *70*, 623.
(39) Varandas, A. J. C.; Rodrigues, S. P. J. *J. Phys. Chem A* **2006**, *110*, 485.
(40) Rodrigues, S. P. J.; Sabín, J. A.; Varandas, A. J. C. *J. Phys. Chem. A* **2002**, *106*, 556.
(41) Martínez-Núñez, E.; Varandas, A. J. C. *J. Phys. Chem. A* **2001**, *105*, 5923.
(42) Varandas, A. J. C.; Rodrigues, S. P. J. *J. Phys. Chem. A* **2007**, *111*, 4869.
(43) Varandas, A. J. C.; Rodrigues, S. P. J. *J. Chem. Phys.* **1997**, *106*, 9647.
(44) Varandas, A. J. C. *J. Mol. Struct. (THEOCHEM)* **1988**, *166*, 59.
(45) Varandas, A. J. C.; Brandão, J.; Quintales, L. A. M. *J. Phys. Chem.* **1988**, *92*, 3732.
(46) Varandas, A. J. C.; Pais, A. A. C. C. *Mol. Phys.* **1988**, *65*, 843.
(47) Rodrigues, S. P. J.; Varandas, A. J. C. *Phys. Chem. Chem. Phys.* **2000**, *2*, 435.
(48) Varandas, A. J. C. In *Conferencias Plenarias de la XXIII Reunion Bienal de Quimica*; Feliciano, A. S., Grande, M., Casado, J., Eds.; Universidad de Salamanca: Salamanca, 1991; p 321.
(49) Martin, J. M. L.; Uzan, O. *Chem. Phys. Lett.* **1998**, *282*, 16.
(50) Dunning, T. H., Jr.; Peterson, K. A; Wilson, A. K. *J. Chem. Phys.* **2001**, *114*, 9244.
(51) Tanimoto, M.; Klaus, T.; Müller, H. S. P.; Winnewisser, G. *J. Mol. Spectrosc.* **2000**, *199*, 73.

(52) Mihelcic, D.; Schindler, R. N. *Ber. Bunsen-Ges. Phys. Chem.* **1970**, *74*, 1280.
(53) Truhlar, D. G. *J. Chem. Phys.* **1972**, *56*, 3189.
(54) Muckerman, J. T.; Newton, M. D. *J. Chem. Phys.* **1972**, *56*, 3191.
(55) Martin, W. C.; Zalubas, R.; Musgrove, A. *J. Phys. Chem. Ref. Data* **1990**, *19*, 821.
(56) Huber, K. P.; Herzberg, G. *Molecular Spectra and Molecular Structure. IV Constants of Diatomic Moleciles*; Van Nostrand: New York, 1979.
(57) Schofield, K. *J. Phys. Chem. Ref. Data* **1973**, *2*, 25.
(58) Nicholas, J. E.; Amodio, C. A.; Baker, M. J. *J. Chem. Soc., Faraday Trans. 1* **1979**, *75*, 1868.
(59) Denis, P. A. *J. Phys. Chem. A* **2004**, *108*, 11092.
(60) Continetti, R. E.; Balko, B. A.; Lee, Y. T. *Chem. Phys. Lett.* **1991**, *182*, 400.
(61) Frederix, P. W. J. M.; Yang, C.-H.; Groenenboom, G. C.; Parker, D. H.; Alnama, K.; Western, C. M.; Orr-Ewing, A. J. *J. Phys. Chem. A* **2009**, *113*, 14995.
(62) Holstein, K. J.; Fink, E. H.; Wildt, J.; Zabel, F. *Chem. Phys. Lett.* **1985**, *113*, 1.
(63) Entfellner, M.; Boesl, U. *Phys. Chem. Chem. Phys.* **2009**, *11*, 2657.